ACS APPLIED MATERIALS & INTERFACES

www.acsami.org

Research Article

Reusable Fluorescent Nanobiosensor Integrated in a Multiwell Plate for Screening and Quantification of Antidiabetic Drugs

Yolanda Alacid, María José Martínez-Tomé, and C. Reyes Mateo*

Cite This: *ACS Appl. Mater. Interfaces* 2021, 13, 25624–25634

Read Online

ACCESS | Metrics & More | Article Recommendations | Supporting Information

ABSTRACT: A highly stable and reusable fluorescent multisample nanobiosensor for the detection of α-glucosidase inhibitors has been developed by coupling fluorescent liposomal nanoparticles based on conjugated polymers (L-CPNs) to the enzyme α-glucosidase, one of the main target enzymes in the treatment of type 2 diabetes. The mechanism of sensing is based on the fluorescence "turn-on" of L-CPNs by *p*-nitrophenol (PNP), the end product of the enzymatic hydrolysis of *p*-nitrophenyl-α-D-glucopyranoside. L-CPNs, composed of lipid vesicles coated with a blue-emitting cationic polyfluorene, were designed and characterized to obtain a good response to PNP. Two nanobiosensor configurations were developed in this study. In the first step, a single-sample nanobiosensor composed of L-CPNs and α-glucosidase entrapped in a sol–gel glass was developed in order to characterize and optimize the device. In the second part, the nanobiosensor was integrated and adapted to a multiwell microplate and the possibility of reusing it and performing multiple measurements simultaneously with samples containing different α-glucosidase inhibitors was investigated. Using super-resolution confocal microscopy, L-CPNs could be visualized within the sol–gel matrix, and the quenching of their fluorescence, induced by the substrate, was directly observed *in situ*. The device was also shown to be useful not only as a platform for screening of antidiabetic drugs but also for quantifying their presence. The latter application was successfully tested with the currently available drug, acarbose.

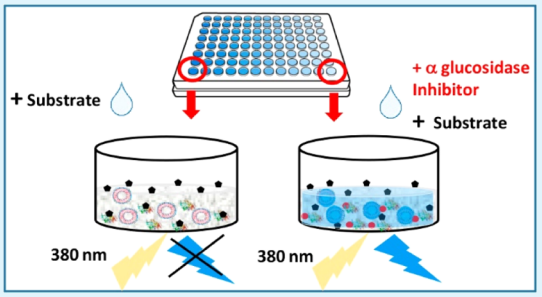

KEYWORDS: *α-glucosidase inhibitors, nanobiosensor, fluorescent conjugated polymers, liposomal nanoparticles, acarbose, multiwell plate, antidiabetic drugs*

INTRODUCTION

Nowadays, medicine is becoming a molecular science in which most drugs are directly targeted toward specific macromolecular sites, whose bioactivity is pathogenic or, at least, associated with the pathology being treated.[1−3] Among the specific macromolecules that can act as therapeutic targets, enzymes occupy a prominent position, given that their catalytic role is essential in many physiological processes. Drugs can act on the enzyme by activating or inhibiting it, the latter being the most common. The use of suitable inhibitors can produce accumulation of the enzyme substrate or a reduction in the products generated. Both effects are interesting from a therapeutic or diagnostic point of view. Therefore, the study of drug-induced enzyme inhibition, the screening of inhibitors, and the monitoring of their toxicity are of great interest in the prevention and treatment of many diseases.[4−6]

One of the most prevalent chronic diseases in the world is diabetes, which is characterized by an abnormal increase in the concentration of glucose in blood. Its complications lead to kidney disorders, blindness, and a marked increase in the risk of heart disease. Type 2 diabetes, or noninsulin-dependent diabetes, is the most common and accounts for 90% of all cases of diabetes. Although there is currently no drug capable of curing this disease, there are treatments that can control it, thus reducing the risks involved.[7,8] One of the most interesting therapeutic approaches for type 2 diabetes is to inhibit the activity of the enzyme α-glucosidase, which converts polysaccharides into absorbable sugars in the intestinal environment. In this way, the digestion of carbohydrates is delayed, reducing the hyperglycemia that occurs after the ingestion of food. Nowadays there are three major drugs in the market belonging to the category of α-glucosidase inhibitors (AGIs): acarbose (the most commonly used AGI), miglitol, and voglibose, although the latter has been discontinued from the US market.[9] These drugs, although efficient, have a very severe dosage regimen and important side effects, mainly gastrointestinal and hepatic, so they are infrequently prescribed in the US and European countries. For this reason, there is increasing interest in finding new antidiabetic agents with

Received: February 5, 2021
Accepted: May 17, 2021
Published: May 27, 2021

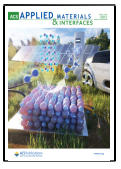

https://doi.org/10.1021/acsami.1c02505
ACS Appl. Mater. Interfaces 2021, 13, 25624–25634

Scheme 1. Schematic Representation and Working Principle of the Single-Sample Nanobiosensor (a) and Multisample Nanobiosensor (b) for Screening of α-Glucosidase Inhibitors, Based on the Quenching (Turn-On) of the Immobilized L-CPNs by PNP, the Enzyme Catalytic Product of PNPG[a]

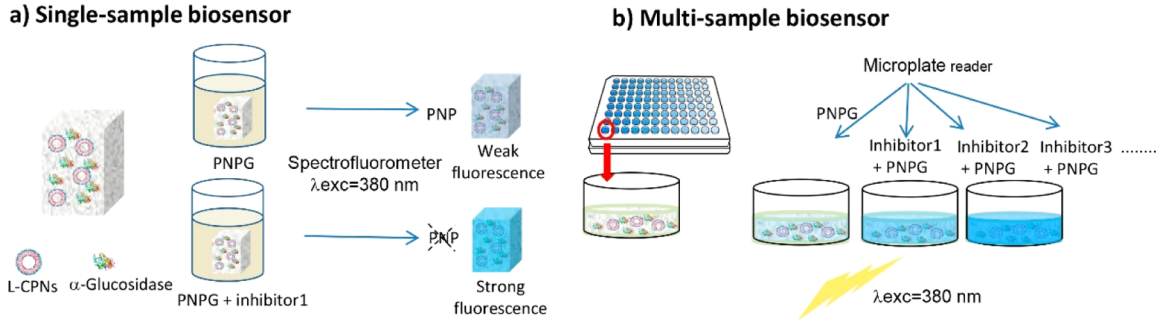

[a]Presence of inhibitors prevents the quenching to a degree that depends on their ability to inhibit α-glucosidase.

better pharmacological profile, capable of inhibiting α-glucosidase, reducing the side effects of current drugs.[8,10,11] However, to date, there has been no significant progress in this field, despite the fact that acarbose and miglitol were introduced in the market in the early 1990s.[12,13]

The identification of new enzyme inhibitors can be carried out, among others, using virtual screening methods, especially if the structure of the enzyme and its active center is known. In this way, a set of compounds that potentially have high affinity and specificity for the active center are selected to behave as competitive inhibitors.[14,15] The screening of inhibitors from traditional Chinese medicines is also a prominent approach of drug discovery. In this sense, many natural products have proved to be a source of compounds that have a high ability to inhibit α-glucosidase.[16] In addition, the synthesis of compounds with a monosaccharide or sugar-mimic frameworks, designed on the basis of the common structure of commercial AGIs, is another strategy in the search for new antidiabetic agents.[11,17] Regardless of the strategy used to identify these new compounds, the next step is to assess their inhibitory activity against α-glucosidase. A recent review summarizes many of the methods developed to date for this purpose.[18] Hyperglycemic animal model for *in vivo* screening and enzyme inhibitor model for *in vitro* screening, using *p*-nitrophenyl-α-D-glucopyranoside (PNPG) as the substrate, are the two most commonly used approaches. However, these tests usually represent a high economic and time cost since they include several stages and the use of enzymes and reactants, which can sometimes be very expensive.[19,20] Specifically, the most commonly used in vitro screening approach is based on a 96-well plate assay using UV−vis spectrophotometry as the detection method. However, numerous sources of error can contribute in affecting the accuracy and reproducibility of these measurements, such as plate edge effects (temperature and evaporation deviations), turbidity, air bubbles during mixing, and so forth, as has been reported in a very recent study.[21] An alternative to conventional methods is the use of enzyme biosensors. These devices are simple, specific, and effective tools for analytical investigations which incorporate an enzyme coupled to a suitable physicochemical transducer, generally optical or electrochemical. In addition, they directly monitor the target enzymes without a complicated pretreatment. In the fabrication of biosensors, the enzyme must be confined/immobilized in an appropriate matrix that does not affect its activity and allows the access of the substrate to the active site, as well as that of possible inhibitors. In past years, various α-glucosidase-based biosensors have been developed to be applied in the screening of potential enzyme inhibitors, the majority of which use colorimetric or electrochemical transducers.[19,20,22,23] New fluorescent strategies are also currently being developed for this purpose, although most of the devices reported are either not reusable because the enzyme and fluorophores are not immobilized or do not allow the simultaneous screening of many compounds, with the consequent economic and time cost.[18,24−26] Therefore, it still remains a challenge to obtain a simple, inexpensive, and reusable platform for α-glucosidase inhibitor screening.

Fluorescent nanoparticles based on conjugated polymers (CPNs) have attracted extensive research interest in recent years because of their low cytotoxicity, excellent photostability, good biocompatibility, and water stability. These excellent properties allow their use as fluorescent probes in biomedical applications such as bioimaging, diagnosis, and drug delivery, without risking the cellular viability.[27−35] In addition, CPNs have received great attention as novel materials in sensing applications, acting as fluorescent transducers for detecting chemical and biological species.[36−38]

Recently, we have developed a "turn-on" fluorescent nanobiosensor for the detection of phosphate ions, an inhibitor of the enzyme alkaline phosphatase (ALP), based on CPNs. For the construction of the device, ALP was coimmobilized in a sol−gel matrix with blue-emitting nanoparticles composed of the cationic polyfluorene, poly{(9,9-bis(6′-*N*,*N*,*N*-trimethylammonium)hexyl]fluorene-phenylene} bromide (HTMA-PFP), incorporated in anionic lipid vesicles.[39] The operating principle of the biosensor is based on the quenching of the fluorescent nanoparticles by *p*-nitrophenol (PNP), the ALP hydrolysis product of the substrate *p*-nitrophenyl phosphate (PNPP). PNP is an electron acceptor that in its anionic form (pK_a = 7.15) quenches the fluorescence of HTMA-PFP, probably through a combination of electron transfer and Förster resonance energy transfer.[25,40] This compound is also the end product of hydrolysis of PNPG, catalyzed by α-glucosidase. Therefore, a fluorescent nanobiosensor for the screening of α-glucosidase inhibitors could be developed by coupling polyfluorene nanoparticles to this enzyme and properly immobilizing the components for easy handling and possible reuse.

In the present work, we have developed a low-cost fluorescent multisample nanobiosensor for the detection of α-glucosidase inhibitors, which potentially could be used as antidiabetic drugs. The device is composed of α-glucosidase

https://doi.org/10.1021/acsami.1c02505
ACS Appl. Mater. Interfaces 2021, 13, 25624−25634

Scheme 2. Scheme of the Fabrication Process (in the Red Box) and Application Procedure of the Multiwell Plate Nanobiosensor for Screening of Antidiabetic drugs; (a): Introduction of the Mixture Composed of L-CPNs and α-Glucosidase in Each Well; (b): Addition of Rotaevaporated Hydrolyzed TEOS; (c): Gelification and Immobilization of the Components; (d): Addition of the Inhibitor; (e): Addition of the Substrate and Measured of Fluorescence from the Bottom of the Wells and Regeneration of the Nanobiosensor after Washing

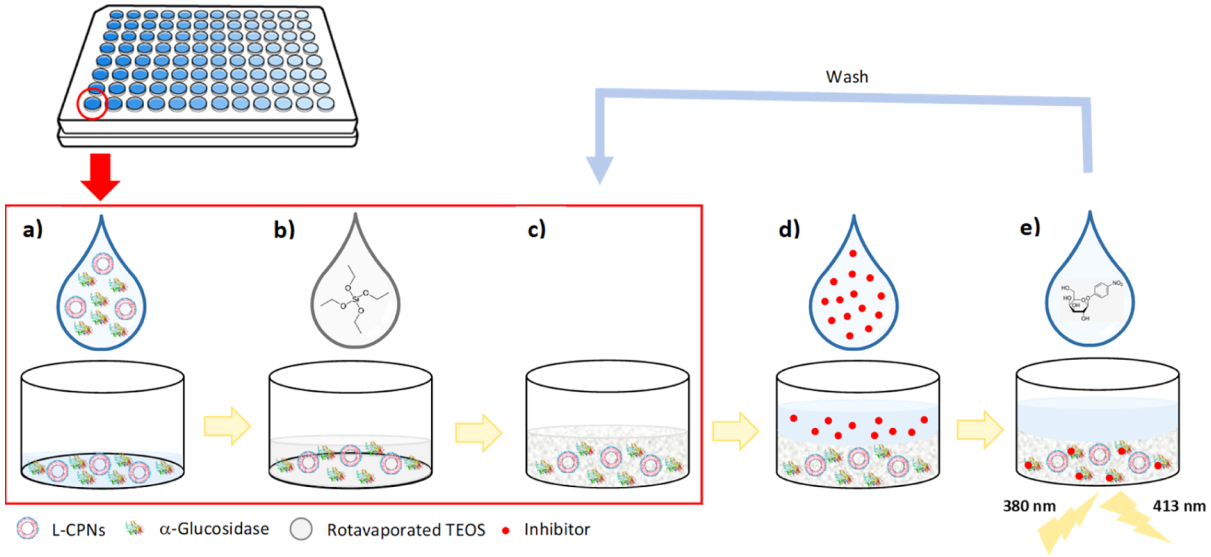

and polyfluorene-liposomal nanoparticles (L-CPNs) immobilized in a sol−gel matrix. In contrast to the previously developed phosphate ion biosensor, which only allows the analysis of one sample per experiment and is therefore not particularly suitable for screening a large number of samples, two different configurations have been developed for the present biosensor (Scheme 1): initially, a single-sample nanobiosensor was tested in a fluorescence cuvette in order to characterize and optimize the device, first with the components in solution and then immobilized in the sol−gel matrix. In the second part, the nanobiosensor was adapted to a 96-well microplate and the ability to be reused and to perform multiple measurements simultaneously, with different inhibitors, was investigated. In addition, using a super-resolution confocal microscope, the immobilized L-CPNs could be individually visualized in the wells and the fluorescence quenching of their fluorescence, induced by the hydrolysis of PNPG, was directly observed *in situ*. Compared to traditional PNPG colorimetric assays, this device has fewer measurement steps and minimizes many of the associated concerns cited above because measurements are made in the solid phase of the wells and not in solution.

MATERIALS AND METHODS

Materials and Reagents. The synthetic phospholipids egg yolk L-α-phosphatidylcholine (PC) and L-α-phosphatidylglycerol sodium salt (PG), enzyme α-glucosidase (E.C. 3.2.1.20, from *Saccharomyces cerevisiae*, ≥10 unit/mg), substrate *p*-nitrophenyl-α-D-glucopyranoside (PNPG) and *p*-nitrophenol (PNP) were obtained from Sigma-Aldrich (Merck Life Science, Madrid, Spain). Stock solutions of α-glucosidase, PNPG, and PNP were dissolved in sodium phosphate buffer (50 mM, 0.1 M NaCl, pH 7.4) at 45.1 μM, 2 mM, and 1 mM, respectively. The polyfluorene HTMA-PFP [M_n (g·mol^{-1}) = 4170; M_w (g·mol^{-1}) = 8340] was synthetized and subsequently characterized in our laboratory.[41−43] Stock solutions of the polyfluorene were prepared in dimethyl sulfoxide (DMSO) with final concentrations of 3.65 × 10^{-4} M (in repeat units) and stored at −20 °C before use. Tetraethyl orthosilicate (TEOS) was obtained from Sigma-Aldrich (Merck Life Science, Madrid, Spain). Sodium phosphate buffer (50 mM, 0.1 M NaCl, pH 7.4) was prepared with twice distilled and deionized water, utilizing Milli-Q equipment (Millipore, Madrid, Spain). Enzyme inhibitors, acarbose, miglitol, and gallic acid were purchased from Alfa Aesar (Thermo Fisher GmbH, Kandel, Germany), Tokyo Chemical Industry Co. Ltd., (Tokyo, Japan) and Merck Life Science (Madrid, Spain), respectively. Stock solution of inhibitors were prepared with sodium phosphate buffer (50 mM, 0.1 M NaCl, pH 7.4) at 100 mM. All other solvents were of spectroscopic or analytical reagent grade (Uvasol, Merck).

Preparation of the Fluorescent Nanoparticles (L-CPNs). Solutions of chloroform containing 2 mg of anionic PG or zwitterionic PC lipids were left to dry under argon gas flow for 20 min. The dried lipid was resuspended in sodium phosphate buffer to the required final concentration (1 mM to limit sample turbidity, a potential artifact in fluorescence measurements) and vortexed several times in order to obtain multilamellar vesicles (MLVs). Large unilamellar vesicles (LUVs) were obtained from MLVs by pressure extrusion through 0.1 μm polycarbonate filters (Nucleopore, Cambridge, MA, USA). Straight away, aliquots of the polyfluorene HTMA-PFP from the stock solution in DMSO were added to the LUVs suspension (final concentration of 3 μM in terms of repeat units) and incubated for at least 30 min at room temperature. The concentration of HTMA-PFP was 3 μM to ensure that all the polymer chains were incorporated into the LUVs, considering the partition coefficient between the lipid and aqueous phase reported previously by our group.[44] The proportion of DMSO in final samples was lower than 1% v/v in all the cases.

Fluorescent Assay of α-Glucosidase in Solution. The functioning of the nanobiosensor was first checked with the components in solution by adding the enzyme to a suspension of L-CPNs and measuring the fluorescence signal after the addition of the substrate. The α-glucosidase concentration in the sample was tested from 0.4 to 1.2 μM (Figure S1). For 0.8 μM, the time necessary to hydrolyze the substrate PNPG (15 μM) and to quench the fluorescence of L-CPNs was ∼13 min, which was considered a good response time for the development of the biosensor in solution. The hydrolysis effect did not improve remarkably when the α-glucosidase concentration was increased to 1.2 μM.

Immobilization of α-Glucosidase and L-CPNs in a Sol−Gel Matrix. Fluorescent L-CPNs and α-glucosidase were first immobilized separately to facilitate their characterization within the sol−gel

https://doi.org/10.1021/acsami.1c02505
ACS Appl. Mater. Interfaces 2021, 13, 25624−25634

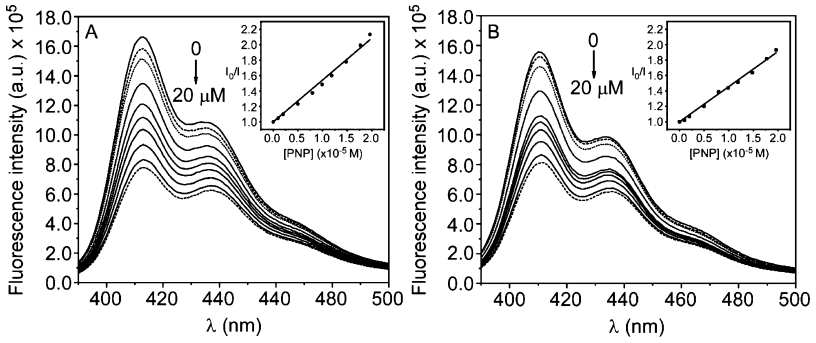

Figure 1. (A) Fluorescence emission spectra of PC and (B) PG L-CPNs at increasing concentrations of PNP (0−20 μM). Inset: Stern−Volmer plot for quenching of HTMA-PFP in LUVs of (A) PC and (B) PG by PNP in sodium phosphate buffer, pH 7.4 (λ_x = 380 nm).

matrix. α-Glucosidase was immobilized by the sol−gel process, as was previously described.[39] In brief, a volume of 4.46 mL of the precursor TEOS was mixed at room temperature with 1.44 mL of H_2O and 0.04 mL of HCl (0.62 M). After stirring for 1 h, 1 mL of this solution was mixed with 1 mL of distilled water and subjected to rotaevaporation to eliminate the alcohol resulting from alkoxide hydrolysis. Immobilized α-glucosidase was prepared by adding 0.7 mL of buffered enzyme (12 μM) solution to 0.7 mL of the rotaevaporated sample. Transparent monoliths containing the α-glucosidase (6 μM) within their pores were rapidly obtained, aged in 1 mL of sodium phosphate buffer during 48 h and stored at 4 °C in the dark before use. The concentration of enzyme was increased to 6 μM in order to obtain a good-quality fluorescence emission spectrum of the protein inside the monolith. In the case of the L-CPNs, the immobilization protocol was similar to that of the enzyme other than adding 0.7 mL of the fluorescent nanoparticle solution (PC/HTMA-PFP, 2 mM:6 μM) to 0.7 mL of the rotaevaporated sample.

Preparation of the α-Glucosidase Nanobiosensor. Two configurations of the nanobiosensor were developed in this work (Scheme 1). For the single-sample nanobiosensor, 0.7 mL of a solution containing L-CPNs (PC/HTMA-PFP, 2 mM:6 μM) and α-glucosidase (12 μM) in sodium phosphate buffer were mixed with 0.7 mL of the rotaevaporated solution in a disposable cuvette. Gelation occurred readily after mixing. The freshly formed monoliths, having a size of ~9 × 9 × 15 mm^3, were aged during 48 h, washed with sodium phosphate buffer, sealed with parafilm and stored in dark at 4 °C. For the multisample device, 75 μL of the buffered nanobiosensor components and 75 μL of the rotaevaporated sample were mixed in the wells of a 96-well microplate. The sol−gel reaction was made directly in the microplate, obtaining solid transparent monoliths of ~150 μL of volume that were fixed at the bottom of the well (Scheme 2). The microplate was sealed with parafilm and stored at 4 °C in the dark before use.

Fluorescence Measurements. For the assays in solution and for the single-sample nanobiosensor, the fluorescence measurements were performed on a PTI-QuantaMaster spectrofluorometer (Birmingham, AL, USA) at 25 °C. Samples were placed in 1 cm-path-length quartz cuvettes and excited at 380 nm. The emission spectra were recorded between 390 and 500 nm (integration time = 0.5 s) using excitation and emission slits of 1 and 1.4 nm, respectively. Background intensities, corresponding to intensities due to the excitation of blanks, were checked and subtracted from the samples. For the biosensor in solution, blanks correspond to suspensions of lipid vesicles (without HTMA-PFP), while for the immobilized biosensor, blanks correspond to sol−gel matrices containing lipid vesicles (without HTMA-PFP). For the multisample nanobiosensor, fluorescence measurements were carried out at 25 °C on a CytationTM3 96-well plate reader (BioTek, Winooski, Vermount, USA). All samples were excited at 380 nm. All measurements in the microplate were made in triplicate. The assessment for statistically significant differences between groups was addressed by performing two-tailed *t*- and ANOVA tests, for two and more groups respectively, at the 95% confidence interval after assessing for normality with the Shapiro−Wilk test.

Fluorescence Quenching Experiments. Fluorescence emissions of the L-CPNs in sodium phosphate buffer were studied in the presence and absence of different PNP and PNPG concentrations. PNP acts as a quencher of the cationic polyfluorene HTMA-PFP through charge or energy transfer process.[39] Stern−Volmer analysis was applied to the obtained fluorescence quenching values according to eq 1

$$I_0/I = 1 + K_{SV}[Q] \quad (1)$$

where, I and I_0 correspond with the steady-state fluorescence intensities in the presence and absence of PNP, respectively, Q represents the quencher concentration, and K_{SV}, the Stern−Volmer constant, whose value gives information on the efficiency of the quenching process and reflects the sensitivity of the fluorophore to the quencher or the accessibility of the fluorophores to a quencher. In the current study, this would describe how easily accessible the polyfluorene (within the L-CPN) is to the PNP compound.

Particle Size and Zeta Potential. The size and zeta potential of L-CPNs were explored by the dynamic light scattering (DLS) technique, with a Malvern Zetasizer Nano-ZS instrument (Worcestershire, UK) equipped with a monochromatic coherent 4 mW helium neon laser (λ = 633 nm) light source, where size measurements were performed at angles of 173°. Size was measured in disposable cuvettes, while zeta potential measurements were performed in specific zeta potential cells. All measurements were carried out in triplicate at room temperature.

Transmission Electron Microscopy. Transmission electron microscopy (TEM) was performed by using a TEM (JEM-1400 Plus, JEOL, Tokyo, Japan), working at 120 kV. Images of LUVs and L-CPNs were obtained by placing a drop of the corresponding suspension on to 300-mesh copper grips coated with carbon film and then stained with lead citrate. These samples were left to air-dry before being placed under the microscope. Digital images were recorded with a Gatan ORIUS camera.

Fluorescence Microscopy. Images of the blue fluorescence of the nanoparticles were acquired with a confocal laser scanning microscope (Zeiss LSM 900 with a super-resolution Airyscan 2 detector) and processed using Carl Zeiss ZEN blue software. L-CPNs were excited at 405 nm and imaged with a 63×/1.4 NA objective (oil-immersion). The image in Figure S2B was taken at Carl Zeiss AG (Oberkochen), and images in Figure 4A,B were acquired at our Institute. Images were analyzed with ImageJ to obtain the corresponding histograms.

RESULTS AND DISCUSSION

Design and Characterization of Fluorescent L-CPNs. Fluorescent L-CPNs were prepared by incorporation of the cationic polyfluorene HTMA-PFP in lipid vesicles (LUVs) composed of zwitterionic (PC) or anionic (PG) lipids, as is described in Materials and Methods. This strategy stabilizes

https://doi.org/10.1021/acsami.1c02505
ACS Appl. Mater. Interfaces 2021, 13, 25624−25634

the polymer, avoiding its high tendency to aggregate in an aqueous environment, which results in a drastic loss of fluorescence intensity.[45] L-CPNs were suspended in buffer at pH 7.4, which is an optimum value for α-glucosidase activity. The choice of the most suitable lipid for the preparation of L-CPNs was made after exploring their ability to be quenched by PNP, the end product of hydrolysis of PNPG. Figure 1A,B shows the fluorescence emission spectra of L-CPNs composed of either PC or PG lipids, respectively, in the absence and in presence of increasing concentrations of PNP (0−20 μM). As expected, a decrease in the fluorescence intensity was observed as the PNP concentration was increased. Two pathways can in principle be responsible for this quenching, and it is difficult to separate them, as described in a previous paper.[39] On the one hand, polyfluorenes are electron donors, while PNP is an electron acceptor, so the fluorescence of HTMA-PFP incorporated in the nanoparticles can be quenched by PNP through a photoinduced electron transfer mechanism. On the other hand, the absorption of PNP, in its anionic form, overlaps with the emission spectrum of HTMA-PFP. Therefore, quenching can take place by a resonance energy transfer process (FRET), from HTMA-PFP to PNP. In any case, although the exact contribution of each mechanism is not known, it was possible to analyze the results by means of Stern−Volmer analysis, as described in Materials and Methods. The corresponding Stern−Volmer plots were linear in the concentration range studied with values of K_{SV} = 5.4 ± 0.1 × 10^4 M^{-1} and K_{SV} = 4.6 ± 0.1 × 10^4 M^{-1} for PC and PG nanoparticles, respectively (inset in Figure 1A,B). These results indicate that both L-CPNs show a fairly similar response to the presence of PNP, although it is slightly higher in the case of the zwitterionic system. The small difference observed may be due to the location of HTMA-PFP in zwitterionic vesicles, which at difference of anionic ones, remains near or at the surface of the bilayer and not in the hydrophobic core.[43,44] This location facilitates the accessibility of PNP to the polymer. Based on these results and considering that a PC lipid, from the point of view of the economic feasibility, is less expensive and more readily available, we selected this phospholipid to make the fluorescent nanoparticles.

The formed nanoparticles were further characterized by DLS and zeta potential measurements to estimate the size and surface charge density (Table 1). The results obtained show

Table 1. Hydrodynamic Diameter (d) and Zeta Potential (ZP) of PC LUVs and L-CPNs

sample	d (nm)	ZP (mV)
PC LUVs	161.5 ± 1.6	6.3 ± 0.7
L-CPNs	164.1 ± 0.5	10.5 ± 0.3

that the hydrodynamic diameter of the L-CPNs is slightly higher than that corresponding to PC LUVs before HTMA-PFP addition, probably because the polymer coats the lipid vesicles. With regard to zeta potential, the polymer helps to stabilize the nanoparticles, although it is still below the optimum value of 30 mV that prevents aggregation over time and promotes colloidal stability.

The size and morphology of the L-CPNs were also explored by TEM experiments. The images of these nanoparticles are shown in Figure S2A. Results indicate that nanoparticles are rather spherical having a size in agreement with those obtained from DLS experiments, taking into account that each technique measures different properties of the sample under different conditions (in DLS, the nanoparticles are suspended in buffer, making them completely hydrated, while for TEM measurements, the samples must be dried and fixed on appropriate media for viewing). Finally, the nanoparticles and their fluorescence emission were viewed individually under the confocal microscopy. L-CPNs were imaged with a 63×/1.4 NA objective (oil-immersion), and their diameters were estimated, obtaining values in the expected range of size (Figure S2B).

Study in Solution of the Nanobiosensor Components. Once the quenching of the fluorescent L-CPNs by PNP was confirmed, it was investigated whether the quenching process was also triggered by the addition of the substrate (PNPG) to a nanoparticle suspension containing the enzyme α-glucosidase. In order to select the incubation time of the assay, a first experiment was performed, in which the fluorescence intensity of the sample was recorded as a function of time upon addition of PNPG 15 μM, in the presence and absence of the enzyme (0.8 μM), as is described in Materials and Methods. The results, displayed in Figure 2A, show that

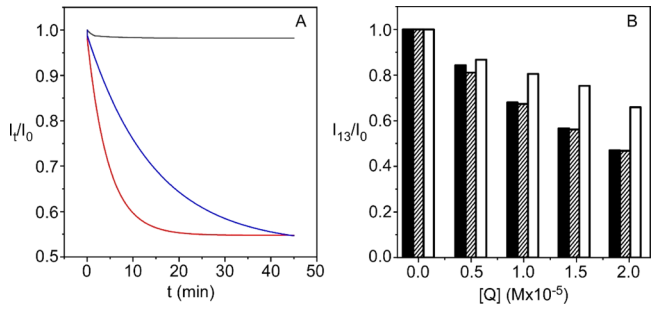

Figure 2. (A) Quenching kinetics of L-CPNs in the absence (black line) and presence of α-glucosidase (0.8 μM) without (red line) and with acarbose (1 mM) (blue line), recorded after addition of PNPG (15 μM). (B) Fluorescence quenching of L-CPNs at increasing concentrations of PNP (black bars) or PNPG in the presence of α-glucosidase (0.8 μM) without (striped bars) and with acarbose 1 mM (white bars), measured before (I_0) and after 13 min of incubation (I_{13}).

the fluorescence quenching, measured as I_t/I_0, where I_t and I_0 are the intensities at time t and 0, respectively, occurs only in the presence of the enzyme and reaches its minimum value around ∼12−15 min, evidencing that the fluorescence of the L-CPNs is able to detect the activity of α-glucosidase. To further confirm this result, increasing concentrations of PNPG (0−20 μM) were added to a sample containing L-CPNs and α-glucosidase, and the corresponding fluorescence spectra were recorded after 13 min of incubation. Figure 2B compares the effect induced on the fluorescence signal of L-CPNs after each addition of the substrate (striped bars), with that obtained by adding the same concentration of PNP (black bars). A similar quenching pattern was observed for both compounds. When the Stern−Volmer analysis was applied to these results, a K_{SV} value of 5.3 ± 0.2 × 10^4 M^{-1} was obtained for PNPG, which similar to that found for PNP.

As described in Introduction, the purpose of this biosensor is to be used as a tool for the screening of α-glucosidase inhibitors (AGIs). The presence of a possible inhibitor in a sample containing L-CPNs and enzyme would prevent the transformation of the substrate into PNP, so that the fluorescence quenching, after the incubation time, would be

https://doi.org/10.1021/acsami.1c02505
ACS Appl. Mater. Interfaces 2021, 13, 25624−25634

less than that observed in its absence. The validity of this potential application was tested using the compound acarbose, which is the first α-glucosidase inhibitor available for treatment of type 2 diabetes. This molecule binds to the active site of the enzyme preventing the hydrolysis of PNPG to PNP. The compound was added to a sample containing L-CPNs and α-glucosidase, and the fluorescence intensity of the nanoparticles was monitored for 45 min upon addition of PNPG 15 μM (blue line in Figure 2A). The results show that the presence of acarbose slowed down the quenching kinetics, obtaining a fluorescence signal, which was clearly higher than that obtained in its absence, especially in the range of 5−20 min incubation time. A similar result was observed at different substrate concentrations. The intensity of fluorescence recorded after 13 min of incubation was higher than that obtained in the absence of the drug (white bars in Figure 2B), evidencing the ability of the nanobiosensor components to detect the presence of AGIs.

Development of the Nanobiosensor: Immobilization of Components. To facilitate the handling and possible reuse of the nanobiosensor components, L-CPNs and α-glucosidase were immobilized in a sol−gel matrix, obtaining solid and transparent glasses whose shape is determined by the container in which the polymerization reaction proceeds. As was mentioned in Introduction, two configurations of the device were developed and tested in this work (Scheme 1): in the first stage, a single-sample nanobiosensor was performed in order to characterize and optimize the device. In the second part, the nanobiosensor was integrated in a multiwell plate and the ability to be reused and to perform multiple measurements simultaneously was investigated.

Single-Sample Nanobiosensor. For this configuration, the biosensor components were immobilized in a sol−gel monolith of ~9 × 9 × 15 mm^3. First, L-CPNs and α-glucosidase were immobilized separately, as is described in Materials and Methods, to check that all the components work properly. In a previous work, our group immobilized L-CPNs prepared with anionic lipids at pH 9.2, reporting that the sol−gel process did not alter the fluorescence properties of the nanoparticles and that they are physically and chemically stable during months.[39] In the present work, the lipid nature of the L-CPNs is different because they are prepared with zwitterionic lipids instead of anionic ones at pH 7.4. For this reason, a similar study was performed, comparing the properties of the immobilized and free L-CPNs. Figure S3A shows the fluorescence spectrum of the immobilized L-CPNs, directly measured from the monolith in the spectrofluorometer. The shape and spectral position of the spectrum was rather similar to that obtained in the buffer. In addition, the intensity of the emission maximum was practically preserved during at least 72 days, reducing their signal by only around 15% (inset in Figure S3A). These results confirm that the immobilization in sol−gel matrices does not only not affect the fluorescent properties of the zwitterionic L-CPNs but also stabilizes the fluorescence signal, probably because it prevents lipid vesicle aggregation.

The next step was to explore if the immobilized L-CPNs are still quenched by PNP. For this experiment, one monolith was immersed in a 5 mL solution containing PNP 20 μM and its fluorescence spectrum was recorded at different incubation times. The intensity of the monolith decreased with time, but the fluorescence signal did not reach a plateau even after 50 min of incubation (Figure S3B). When the PNP concentration was increased, the quenching of fluorescence was much faster, reaching its minimum value around 50 and 30 min for concentrations of 500 and 1000 μM, respectively. This behavior was attributed to the diffusion restrictions imposed by the porous matrix that limit the accessibility of small molecules to the nanoparticles and has been previously reported for PNP and other analytes in sol−gel glasses.[39,46] These results show that the immobilized L-CPNs can be quenched by PNP, although with slower kinetics than that observed in solution and therefore confirm their possible use in the detection of α-glucosidase inhibitors.

Despite the relevance of α-glucosidase, there are hardly any studies in which this enzyme has been immobilized and characterized in sol−gel matrices. In this work, immobilization was confirmed from the intrinsic fluorescence of the protein, mainly due to its tryptophan residues. The fluorescence of these residues occurs at ~334 nm, and is highly sensitive to the polarity of their environment, shifting to 347 nm during urea denaturation.[47] Figure S4 shows the fluorescence spectra of the enzyme in buffer and entrapped in the monolith. The peak observed at ~334 nm and the shape of the spectrum were preserved after sol−gel immobilization, suggesting that the enzyme has been successfully immobilized without altering its structural conformation.

After L-CPNs and α-glucosidase were successfully encapsulated separately, both components were coimmobilized in the same monolith, as is described in Materials and Methods, to obtain the final form of the nanobiosensor. In order to check its functioning, the monolith was incubated in a solution containing PNPG 500 μM and its fluorescence spectra were recorded at different times and compared with those obtained after incubation in a PNP 500 μM solution. The emission maximum intensity for each time is drawn in Figure 3 (red

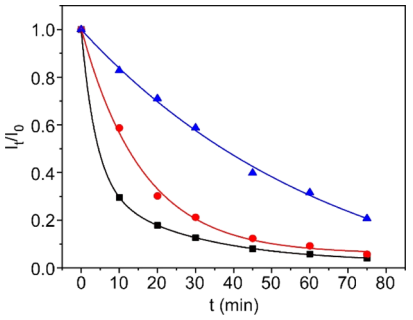

Figure 3. Fluorescence quenching kinetics (I_t/I_0) of immobilized L-CPNs measured in the monolith after its immersion in a solution containing 500 μM PNP (black squares) or PNPG without (red circles) and with acarbose 10 mM (blue triangles) (λ_x = 380 nm; λ_m = 413 nm).

circles and black squares for PNPG and PNP, respectively). The decrease of fluorescence indicates that the hydrolysis of PNPG is taking place, confirming the suitability of the coimmobilization process and the ability of the biosensor to detect α-glucosidase activity. It is of interest to note that the quenching kinetics was slower than that observed when the monolith was directly incubated in the presence of PNP 500 μM. This result was expected because PNPG has to diffuse through the sol−gel matrix to reach the enzyme molecules and produce PNP.

Finally, we explored the ability of the biosensor to detect the presence of AGIs. With this end, the monolith was previously incubated in a solution of acarbose 10 mM for at least 3 h to guarantee the access of the inhibitor to the enzyme and

https://doi.org/10.1021/acsami.1c02505
ACS Appl. Mater. Interfaces 2021, 13, 25624−25634

subsequently immersed in a solution containing PNPG 500 μM. Fluorescence spectra were recorded at different incubation times, and the fluorescence intensity in the emission maximum was compared to that obtained in the absence of acarbose. Blue triangles in Figure 3 show that the fluorescence quenching is much less efficient for the monolith exposed to acarbose. Incubation times of 10−20 min are sufficient to detect its presence. This result indicates that the biosensor is able to detect whether a given compound is an inhibitor of α-glucosidase and can therefore be used as a tool for the screening of α-glucosidase inhibitors.

Multisample Nanobiosensor. The above device allows testing only one sample per experiment, thus increasing the time and cost of the assay when more than one compound is to be tested. In addition, the device is fragile because for each test, it is necessary to immerse the biosensor previously in the sample and then, after the incubation time, remove it to measure its fluorescence signal. This procedure can produce small breaks in the sol−gel matrix that affect the measured intensity. In order to develop a more effective and robust method able to analyze multiple samples in one only assay, the single nanobiosensor was adapted to a 96-well microplate that allows the simultaneous screening of a large number of samples and can be reused. The new format also has the advantage of minimizing the sample volume and the reagents used (Scheme 2).

With this end, the nanobiosensor components, L-CPNs and α-glucosidase, were coimmobilized, directly leading to the sol−gel reaction in the wells of the microplate, as is described in Materials and Methods and illustrated in Scheme 2. In the first experiment, we explored the fluorescence intensity and stability of the monoliths as a function of storage time. The analysis of the fluorescence emitted was carried out simultaneously for all the wells containing the immobilized L-CPNs and the measurements were taken in the plate reader from the bottom of the wells. The microplate was stored in darkness in the fridge (4 °C), and the intensity of these wells was recorded for 40 weeks (Figure S5). The results show that the signal is preserved during, at least, this period of time, suggesting that their stability is even greater than that observed for the largest monoliths.

In order to better characterize the multisample nanobiosensor, one of the monoliths was directly observed under the confocal microscope described in Materials and Methods (Figure 4A). The immobilized blue-emitting L-CPNs could be viewed individually, and their size was comparable to that determined in solution (Figure S2B). This result suggests that the nanoparticles do not aggregate during the sol−gel process and remain confined in each pore, which could explain their high stability over time.[48] The advantage of having the L-CPNs immobilized is that it allows to visualize the same nanoparticles after a certain time. This allowed us to check the functioning of the biosensor at a submicroscopic level. Figure 4B shows the image of the same field captured after 1 h PNPG (500 μM) treatment. Histograms and 2.5D plots corresponding to these images are shown in the Supporting Information (Figure S6). The results show that some of the fluorescent L-CPNs visualized in Figure 4A are still visible after the addition of PNPG, but many of them are totally quenched, therefore evidencing the adequate activity of the immobilized enzyme. The fact that some L-CPNs are only partially quenched (as deduced from 2.5D plots) could be due to the different accessibility of the PNP molecules to the pore in which the nanoparticle is entrapped and the fact that each nanoparticle contains more than one fluorophore group (fluorescent polymer chain). Probably, not all the pores are equally accessible to the PNP molecules nor are they exactly the same size, so in some of them the PNP will arrive earlier and its concentration will be higher, being able to completely quench the fluorescence of the nanoparticle, while in the less accessible ones, the concentration will be lower, and it will only be able to quench some of the fluorescent chains present in the nanoparticle. If more PNPG was added and the incubation time increased, all nanoparticles would be fully quenched, as deduced from Figure S3B.

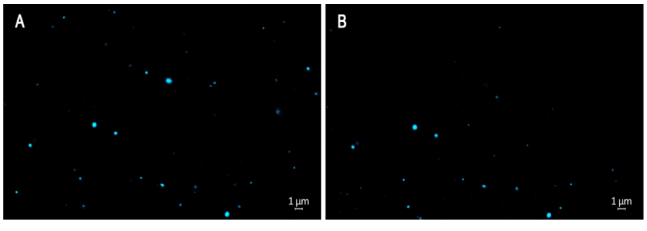

Figure 4. (A) Confocal fluorescence microscopy images of L-CPNs immobilized in a sol−gel matrix before and (B) after 1 h PNPG (500 μM) treatment. Both images correspond to the same field.

To select the operating conditions of the nanobiosensor, a solution of 150 μL of PNPG (500 μM) was added to the wells of the microplate and their fluorescence intensity was measured at different incubation times in the plate reader (Figure 5A). The decrease of the fluorescence signal confirmed the suitability of the device to detect the activity of α-glucosidase, as previously observed by fluorescence microscopy. It should be noted that the time response to PNPG is slower than that observed in the single-sample device. This result was to be expected because, unlike the single-sample biosensor, in which the monolith is completely immersed in a PNPG solution, in the new device, the monoliths are attached to the wells so that only their surface is in contact with the substrate solution, and the PNPG molecules have more difficulty reaching the active site of the enzyme. Figure 5A shows that for a concentration of the substrate of 500 μM, ∼50% of fluorescence quenching is obtained after 1 h of incubation, a response time that we consider acceptable for the use of the nanobiosensor.

To prove that the device could be reused on more than one occasion, the same microplate of the above experiment was used in three additional assays. In each assay, 500 μM PNPG was added to the wells and the fluorescence intensity was measured after 1 h of incubation. The signal was compared to that of the first assay (Figure 5B). After each assay, the microplate was washed with phosphate buffer for 3 h, changing the buffer every hour to remove the residual PNP. The fact that the quenching efficiency does not differ significantly in all four assays shows that the device can be used at least four times without loss of sensitivity.

In addition to exploring the reuse of the device, we also tested whether the nanobiosensor response was maintained after a long period of storage. For this purpose, a microplate was stored for 10 months in the refrigerator, and after this period of time, the fluorescence signal was measured before and 1 h after the addition of PNPG (500 μM). The intensity recovered was practically similar to that obtained when the

https://doi.org/10.1021/acsami.1c02505
ACS Appl. Mater. Interfaces 2021, 13, 25624−25634

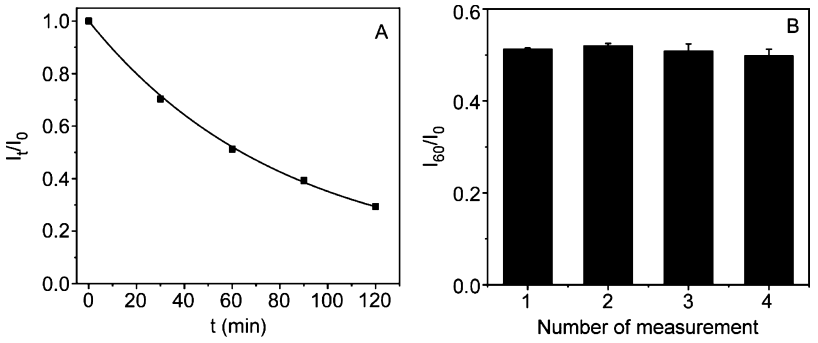

Figure 5. (A) Fluorescence quenching as a function of time (I_t/I_0) recorded from the wells of the multisample biosensor (λ_x = 380 nm; λ_{em} = 413 nm) after addition of 150 μL of PNPG (500 μM). (B) Reusability of the multisample biosensor tested using the same microplate for three additional assays, measuring the fluorescence decrease percentage after 60 min of incubation (I_{60}/I_0). Each column represents three replicates and error bar stands for standard deviation (SD) of the mean.

nanobiosensor was recently prepared (Figure S7), evidencing the large stability of the device.

Finally, the ability of the multisample nanobiosensor to detect AGIs was checked using acarbose. First, the wells were previously incubated for at least 3 h with 150 μL of a solution containing increasing concentrations of the drug (from 0 to 10 mM). Then, the solution was removed and an equivalent volume of PNPG (500 μM) was added to each well and its fluorescence intensity was recorded before and after 1 h of incubation (Figure S8). The results show that as the concentration of acarbose increases, the quenching efficiency decreases, evidencing that the device is able to detect the effect of the inhibitor. To confirm that the biosensor, after washing, did not lose sensitivity to the inhibitor, the assay was repeated with the same concentrations of acarbose. The results were not significantly different from those of the first test (Figure S8), which again demonstrates the capacity of the nanobiosensor to be reused.

Applications of the Multisample Nanobiosensor. Once the multisample nanobiosensor was characterized and its capacity to be reused and to detect the presence of acarbose was confirmed, it was used to explore the inhibitory capacity of several compounds simultaneously. With this end, four series of wells were previously incubated with 150 μL of buffer, acarbose, miglitol, and gallic acid at different concentrations (10, 20, and 50 mM) and the fluorescence decrease percentage was measured 60 min after addition of 500 μM PNPG (Figure 6). The fluorescence of the control (without inhibitor) was subtracted to better show the ability of the compounds to inactivate the enzyme. Results show that all three compounds are inhibitors of α-glucosidase, but acarbose has the highest effectiveness. Miglitol is the second α-glucosidase inhibitor approved for the treatment of type 2 diabetes. Previous works have reported that its inhibitory capacity is lower than that of acarbose,[49] which agrees with our results. The third compound, gallic acid, has recently been proposed as a potential inhibitor of this enzyme, alone or combined with acarbose.[50,51] The results displayed in Figure 6 support this finding and show that its inhibitory activity does not significantly differ from that of miglitol.

In addition to detecting the presence of AGIs, results shown in Figures S8 and 6 suggest that the nanobiosensor could also be used to estimate their concentration. This potential application was checked for acarbose. Few analytical methods have been reported for the estimation of this compound in pharmaceutical formulation. This information is of interest

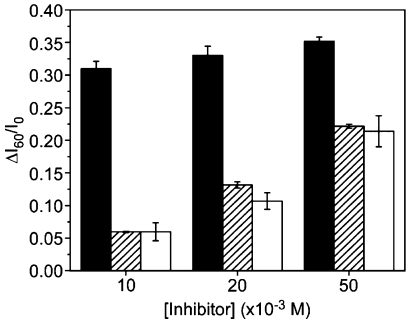

Figure 6. Effect of different inhibitor concentrations (acarbose, black bar; miglitol, striped bar; and gallic acid, white bar) on the fluorescence quenching of the multisample nanobiosensor measured 60 min after addition of 150 μL of PNPG (500 μM) (λ_x = 380 nm; λ_{em} = 413 nm). The fluorescence of the control (without inhibitor) was subtracted to better show the effect of the inhibitor (ΔI_{60} = $I_{60}^{+inhibitor} - I_{60}^{-inhibitor}$). Note: the x-axis is not to scale.

among others for the good manufacturing practice of pharmaceuticals products and is currently performed by HPLC.[52] To carry out this study, the wells of the multisample biosensor were previously incubated with 150 μL of buffer and increasing concentrations of acarbose (up to 3 mM). Once the solution was removed, the same concentration of PNPG (500 μM) was added to all the wells and their fluorescence intensity was measured before and after 60 min of incubation. Figure 7 shows the calibration curve corresponding to this inhibitor. At

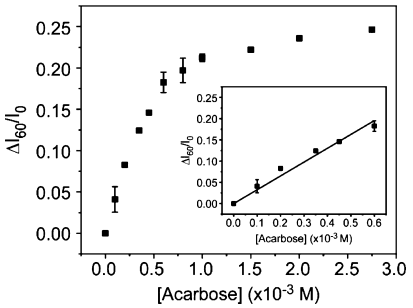

Figure 7. Acarbose calibration curve. The fluorescence intensities were measured at the bottom of the wells 60 min after the addition of PNPG (500 μM). Inset: linear section of the acarbose calibration curve. The intensity values in the y axis are the final values obtained after subtraction of the fluorescence corresponding to the wells in the absence of the inhibitor $\Delta I_{60}/I_0$.

https://doi.org/10.1021/acsami.1c02505
ACS Appl. Mater. Interfaces 2021, 13, 25624−25634

low concentrations, the response is rather linear up to ∼500 μM (inset in Figure 7) with a limit of detection (LOD) of 37.8 μM, calculated from the following equation: LOD = $3\sigma/S$, where S is the slope of the calibration curve and σ is the standard deviation of the blank (sol−gel matrix in the absence of fluorophores). This value is 4 times lower than that recently determined for the colorimetric 96-well plate assay, once optimized and validated.[53] These parameters suggest that the developed nanobiosensor could be a simpler, more cost-effective, and faster alternative to the current methods used for the determination and stability test of acarbose in bulk or pharmaceutical dosage forms.[52]

CONCLUSIONS

In the present work, we have developed a highly stable fluorescent nanobiosensor for the detection of α-glucosidase inhibitors, which is based on the quenching of polyfluorene-liposomal nanoparticles (L-CPNs) by PNP, the enzyme catalytic product of PNPG. The presence of inhibitors prevents the quenching to a degree that depends on their ability to inhibit the enzyme α-glucosidase, which is coimmobilized together with the L-CPNs within a sol−gel matrix. The substrate-induced fluorescence quenching of individual L-CPNs can be observed directly *in situ* under confocal fluorescence microscopy. The strength of this device is based on the adaptation of the nanobiosensor to a 96-well microplate that allows the simultaneous screening of a large number of compounds that potentially could be used as antidiabetic drugs. Compared to the traditional colorimetric assay with PNPG, this device has fewer measurement steps, is easy to handle, and minimizes potential sources of error that occur when measurements are made in solution. With this nanobiosensor, since the sol−gel matrices are transparent and have a porosity that does not allow leaching of the nanoparticles or enzyme but does allow diffusion of the substrate/inhibitor, the measurement can be performed directly in the solid phase. Moreover, since the change in fluorescence signal is reversible, the plate can be reused after washing and stored for at least 10 months.

The ability of the nanobiosensor to determine the concentration of a specific inhibitor has also been demonstrated. The device was successfully applied for the determination of acarbose in an aqueous sample, with a LOD of 37.8 μM, which suggests that it could be used not only as a platform for screening of antidiabetic drugs but also as a simple, cost-effective, and fast tool for routine quality control of acarbose tablets.

ASSOCIATED CONTENT

Supporting Information

The Supporting Information is available free of charge at https://pubs.acs.org/doi/10.1021/acsami.1c02505.

Effect of enzyme concentration on quenching kinetics; TEM and fluorescence microscopy of LCPNs in solution; characterization/stability of L-CPNs and α-glucosidase in sol−gel matrix; histograms and 2.5D plots of fluorescence microscopy images; and capacity of the nanobiosensor to detect acarbose and to be reused (PDF)

AUTHOR INFORMATION

Corresponding Author

C. Reyes Mateo − *Instituto de Investigación, Desarrollo e Innovación en Biotecnología Sanitaria de Elche, Universidad Miguel Hernández, Elche 03202, Alicante, Spain;* orcid.org/0000-0002-2085-1676; Email: rmateo@umh.es

Authors

Yolanda Alacid − *Instituto de Investigación, Desarrollo e Innovación en Biotecnología Sanitaria de Elche, Universidad Miguel Hernández, Elche 03202, Alicante, Spain*

María José Martínez-Tomé − *Instituto de Investigación, Desarrollo e Innovación en Biotecnología Sanitaria de Elche, Universidad Miguel Hernández, Elche 03202, Alicante, Spain*

Complete contact information is available at: https://pubs.acs.org/10.1021/acsami.1c02505

Notes

The authors declare no competing financial interest.

ACKNOWLEDGMENTS

This work was supported by project MAT-2017-86805-R from the Spanish Ministry of Economy, Industry, and Competitiveness. C.R.M. and M.J.M. received funding for equipment from the Generalitat Valenciana - Conselleria d'Educació Investigació Cultura i Esport and EU-FEDER "Una forma de hacer Europa" (GVA-IDIFEDER 2018/020) and Ministry of Science and Innovation and EU-FEDER through the project EQC2019-005842-P. The authors thank Dr. Frank Vogler at Carl Zeiss AG (Oberkochen) for confocal fluorescence microscopy measurements.

REFERENCES

(1) Copeland, R. A.; Harpel, M. R.; Tummino, P. J. Targeting enzyme inhibitors in drug discovery. *Expert Opin. Ther. Targets* **2007**, *11*, 967−978.

(2) Na, I.; Choi, S.; Son, S. H.; Uversky, V. N.; Kim, C. G. Drug Discovery Targeting the Disorder-To-Order Transition Regions through the Conformational Diversity Mimicking and Statistical Analysis. *Int. J. Mol. Sci.* **2020**, *21*, 5248.

(3) Chan, H. C. S.; Shan, H.; Dahoun, T.; Vogel, H.; Yuan, S. Advancing Drug Discovery via Artificial Intelligence. *Trends Pharmacol. Sci.* **2019**, *40*, 592−604.

(4) Holdgate, G. A.; Meek, T. D.; Grimley, R. L. Mechanistic enzymology in drug discovery: a fresh perspective. *Nat. Rev. Drug Discov.* **2018**, *17*, 115−132.

(5) Copeland, R. A. Evaluation of enzyme inhibitors in drug discovery. A guide for medicinal chemists and pharmacologists. *Methods Biochem. Anal.* **2005**, *46*, 1−265.

(6) El Harrad, L.; Bourais, I.; Mohammadi, H.; Amine, A. Recent Advances in Electrochemical Biosensors Based on Enzyme Inhibition for Clinical and Pharmaceutical Applications. *Sensors* **2018**, *18*, 164.

(7) Meneses, M.; Silva, B.; Sousa, M.; Sá, R.; Oliveira, P.; Alves, M. Antidiabetic Drugs: Mechanisms of Action and Potential Outcomes on Cellular Metabolism. *Curr. Pharm. Des.* **2015**, *21*, 3606−3620.

(8) Kerru, N.; Singh-Pillay, A.; Awolade, P.; Singh, P. Current anti-diabetic agents and their molecular targets: A review. *Eur. J. Med. Chem.* **2018**, *152*, 436−488.

(9) Hedrington, M. S.; Davis, S. N. Considerations when using alpha-glucosidase inhibitors in the treatment of type 2 diabetes. *Expet Opin. Pharmacother.* **2019**, *20*, 2229−2235.

(10) Dhameja, M.; Gupta, P. Synthetic heterocyclic candidates as promising α-glucosidase inhibitors: An overview. *Eur. J. Med. Chem.* **2019**, *176*, 343−377.
(11) Liu, H.; Li, M.; Xia, Y.; Ren, X. A Turn-On Fluorescent Sensor for Selective and Sensitive Detection of Alkaline Phosphatase Activity with Gold Nanoclusters Based on Inner Filter Effect. *ACS Appl. Mater. Interfaces* **2017**, *9*, 120−126.
(12) Ghani, U. Re-exploring promising alpha-glucosidase inhibitors for potential development into oral anti-diabetic drugs: Finding needle in the haystack. *Eur. J. Med. Chem.* **2015**, *103*, 133−162.
(13) Barakat, A.; Islam, M. S.; Al-Majid, A. M.; Soliman, S. M.; Ghabbour, H. A.; Yousuf, S.; Choudhary, M. I.; Ul-Haq, Z. Synthesis, molecular structure, spectral analysis, and biological activity of new malonamide derivatives as α-glucosidase inhibitors. *J. Mol. Struct.* **2017**, *1134*, 253−264.
(14) Rahman, N.; Muhammad, I.; Gul-E-Nayab, H.; Khan, M.; Aschner, R.; Filosa, M.; Daglia, fnm Molecular Docking of Isolated Alkaloids for Possible α-Glucosidase Inhibition. *Biomolecules* **2019**, *9*, 544.
(15) Zhu, J.; Zhang, B.; Tan, C.; Huang, Q. α-Glucosidase inhibitors: consistency of in silico docking data with in vitro inhibitory data and inhibitory effect prediction of quercetin derivatives. *Food Funct.* **2019**, *10*, 6312−6321.
(16) Xiong, Y.; Liu, Q.; Yin, X. Synthesis of α-glucosidase-immobilized nanoparticles and their application in screening for α-glucosidase inhibitors. *J. Chromatogr. B: Anal. Technol. Biomed. Life Sci.* **2016**, *1022*, 75−80.
(17) Knudsen, I. M. B.; Hedberg, C.; Ladefoged, L. K.; Ide, D.; Brinkø, A.; Eikeland, E. Z.; Kato, A.; Jensen, H. H. Divergent synthesis of new α-glucosidase inhibitors obtained through a vinyl Grignard-mediated carbocyclisation. *Org. Biomol. Chem.* **2018**, *16*, 6250−6261.
(18) Zhang, X.; Li, G.; Wu, D.; Yu, Y.; Hu, N.; Wang, H.; Li, X.; Wu, Y. Emerging strategies for the activity assay and inhibitor screening of alpha-glucosidase. *Food Funct.* **2020**, *11*, 66−82.
(19) Zhong, Y.; Yu, L.; He, Q.; Zhu, Q.; Zhang, C.; Cui, X.; Zheng, J.; Zhao, S. Bifunctional Hybrid Enzyme-Catalytic Metal Organic Framework Reactors for α-Glucosidase Inhibitor Screening. *ACS Appl. Mater. Interfaces* **2019**, *11*, 32769−32777.
(20) Li, J.; He, G.; Wang, B.; Shi, L.; Gao, T.; Li, G. Fabrication of reusable electrochemical biosensor and its application for the assay of α-glucosidase activity. *Anal. Chim. Acta* **2018**, *1026*, 140−146.
(21) Lankatillake, C.; Luo, S.; Flavel, M.; Lenon, G. B.; Gill, H.; Huynh, T.; Dias, D. A. Screening natural product extracts for potential enzyme inhibitors: protocols, and the standardisation of the usage of blanks in α-amylase, α-glucosidase and lipase assays. *Plant Methods* **2021**, *17*, 3.
(22) Chen, H.; Zhang, J.; Wu, H.; Koh, K.; Yin, Y. Sensitive colorimetric assays for α-glucosidase activity and inhibitor screening based on unmodified gold nanoparticles. *Anal. Chim. Acta* **2015**, *875*, 92−98.
(23) Mohiuddin, M.; Arbain, D.; Islam, A. K.; Ahmad, M. S.; Ahmad, M. N. Alpha-Glucosidase Enzyme Biosensor for the Electrochemical Measurement of Antidiabetic Potential of Medicinal Plants. *Nanoscale Res. Lett.* **2016**, *11*, 95.
(24) Li, G.; Kong, W.; Zhao, M.; Lu, S.; Gong, P.; Chen, G.; Xia, L.; Wang, H.; You, J.; Wu, Y. A fluorescence resonance energy transfer (FRET) based "Turn-On" nanofluorescence sensor using a nitrogen-doped carbon dot-hexagonal cobalt oxyhydroxide nanosheet architecture and application to α-glucosidase inhibitor screening. *Biosens. Bioelectron.* **2016**, *79*, 728−735.
(25) Cao, A.; Tang, Y.; Liu, Y. Novel fluorescent biosensor for α-glucosidase inhibitor screening based on cationic conjugated polymers. *ACS Appl. Mater. Interfaces* **2012**, *4*, 3773−3778.
(26) Liu, J.; Duan, X.; Wang, M.; Su, X. A label-free fluorescent sensor based on silicon quantum dots-MnO(2) nanosheets for the detection of α-glucosidase and its inhibitor. *Analyst* **2019**, *144*, 7398−7405.
(27) MacFarlane, L. R.; Shaikh, H.; Garcia-Hernandez, J. D.; Vespa, M.; Fukui, T.; Manners, I. Functional nanoparticles through π-conjugated polymer self-assembly. *Nat. Rev. Mater.* **2021**, *6*, 7−26.
(28) Lu, Z.; Zhang, Z.; Tang, Y. Conjugated Polymers-Based Thermal-Responsive Nanoparticles for Controlled Drug Delivery, Tracking and Synergistic Photodynamic Therapy/Chemotherapy. *ACS Appl. Bio Mater.* **2019**, *2*, 4485−4492.
(29) Kim, S.; Lim, C.-K.; Na, J.; Lee, Y.-D.; Kim, K.; Choi, K.; Leary, J. F.; Kwon, I. C. Conjugated polymer nanoparticles for biomedical in vivo imaging. *Chem. Commun.* **2010**, *46*, 1617−1619.
(30) Feng, L.; Zhu, C.; Yuan, H.; Liu, L.; Lv, F.; Wang, S. Conjugated polymer nanoparticles: preparation, properties, functionalization and biological applications. *Chem. Soc. Rev.* **2013**, *42*, 6620−6633.
(31) Feng, G.; Liu, J.; Liu, R.; Mao, D.; Tomczak, N.; Liu, B. Ultrasmall Conjugated Polymer Nanoparticles with High Specificity for Targeted Cancer Cell Imaging. *Adv. Sci.* **2017**, *4*, 1600407.
(32) Liu, J.; Li, K.; Liu, B. Far-Red/Near-Infrared Conjugated Polymer Nanoparticles for Long-Term In Situ Monitoring of Liver Tumor Growth. *Adv. Sci.* **2015**, *2*, 1500008.
(33) Wang, Y.; Li, S.; Zhang, P.; Bai, H.; Feng, L.; Lv, F.; Liu, L.; Wang, S. Photothermal-Responsive Conjugated Polymer Nanoparticles for Remote Control of Gene Expression in Living Cells. *Adv. Mater.* **2018**, *30*, 1705418.
(34) Wang, L.; Zhao, Q.; Zhang, Z.; Lu, Z.; Zhao, Y.; Tang, Y. Fluorescent Conjugated Polymer/Quarternary Ammonium Salt Co-assembly Nanoparticles: Applications in Highly Effective Antibacteria and Bioimaging. *ACS Appl. Bio Mater.* **2018**, *1*, 1478−1486.
(35) Rubio-Camacho, M.; Alacid, Y.; Mallavia, R.; Martínez-Tomé, M. J.; Mateo, C. R. Polyfluorene-Based Multicolor Fluorescent Nanoparticles Activated by Temperature for Bioimaging and Drug Delivery. *Nanomaterials* **2019**, *9*, 1485.
(36) Liu, Y.; Wang, Y.-M.; Zhu, W.-Y.; Zhang, C.-H.; Tang, H.; Jiang, J.-H. Conjugated polymer nanoparticles-based fluorescent biosensor for ultrasensitive detection of hydroquinone. *Anal. Chim. Acta* **2018**, *1012*, 60−65.
(37) Childress, E. S.; Roberts, C. A.; Sherwood, D. Y.; LeGuyader, C. L. M.; Harbron, E. J. Ratiometric fluorescence detection of mercury ions in water by conjugated polymer nanoparticles. *Anal. Chem.* **2012**, *84*, 1235−1239.
(38) Roy, S.; Gunukula, A.; Ghosh, B.; Chakraborty, C. A folic acid-sensitive polyfluorene based "turn-off" fluorescence nanoprobe for folate receptor overexpressed cancer cell imaging. *Sens. Actuators, B* **2019**, *291*, 337−344.
(39) Kahveci, Z.; Martínez-Tomé, M. J.; Mallavia, R.; Mateo, C. R. Fluorescent Biosensor for Phosphate Determination Based on Immobilized Polyfluorene-Liposomal Nanoparticles Coupled with Alkaline Phosphatase. *ACS Appl. Mater. Interfaces* **2017**, *9*, 136−144.
(40) Naeem, A.; Khan, I. M.; Ahmad, A. Spectral investigations of multiple charge transfer complex of p-nitrophenol as an electron acceptor with donor p-dimethylaminobenzaldehyde. *Russ. J. Phys. Chem. A* **2011**, *85*, 1840−1843.
(41) Molina, R.; Gómez-Ruiz, S.; Montilla, F.; Salinas-Castillo, A.; Fernández-Arroyo, S.; Ramos, M. d. M.; Micol, V.; Mallavia, R. Progress in the Synthesis of Poly(2,7-Fluorene-*alt*-1,4-Phenylene), PFP, via Suzuki Coupling. *Macromolecules* **2009**, *42*, 5471−5477.
(42) Mallavia, R.; Martínez-Pérez, D.; Chmelka, B. F.; Bazan, G. C. Películas fluorescentes azules basadas en derivados de poli-2,7-fluorenofenilideno. *Bol. Soc. Esp. Ceram. Vidrio* **2011**, *43*, 327−330.
(43) Kahveci, Z.; Martínez-Tomé, M.; Esquembre, R.; Mallavia, R.; Mateo, C. Selective Interaction of a Cationic Polyfluorene with Model Lipid Membranes: Anionic versus Zwitterionic Lipids. *Materials* **2014**, *7*, 2120−2140.
(44) Kahveci, Z.; Vázquez-Guilló, R.; Mira, A.; Martinez, L.; Falcó, A.; Mallavia, R.; Mateo, C. R. Selective recognition and imaging of bacterial model membranes over mammalian ones by using cationic conjugated polyelectrolytes. *Analyst* **2016**, *141*, 6287−6296.
(45) Kahveci, Z.; Martínez-Tomé, M. J.; Mallavia, R.; Mateo, C. R. Use of the Conjugated Polyelectrolyte Poly{[9,9-bis(6′-N,N,N-

https://doi.org/10.1021/acsami.1c02505
ACS Appl. Mater. Interfaces 2021, 13, 25624−25634

trimethylammonium)hexyl]fluorene-phenylene} Bromide (HTMA-PFP) as a Fluorescent Membrane Marker. *Biomacromolecules* **2013**, *14*, 1990−1998.
(46) Pastor, I.; Esquembre, R.; Micol, V.; Mallavia, R.; Mateo, C. R. A ready-to-use fluorimetric biosensor for superoxide radical using superoxide dismutase and peroxidase immobilized in sol-gel glasses. *Anal. Biochem.* **2004**, *334*, 335−343.
(47) Wu, X.-Q.; Wang, J.; Lü, Z.-R.; Tang, H.-M.; Park, D.; Oh, S.-H.; Bhak, J.; Shi, L.; Park, Y.-D.; Zou, F. Alpha-glucosidase folding during urea denaturation: enzyme kinetics and computational prediction. *Appl. Biochem. Biotechnol.* **2010**, *160*, 1341−1355.
(48) Esquembre, R.; Pinto, S. N.; Poveda, J. A.; Prieto, M.; Mateo, C. R. Immobilization and characterization of giant unilamellar vesicles (GUVs) within porous silica glasses. *Soft Matter* **2012**, *8*, 408−417.
(49) Kasturi, S.; Surarapu, S.; Uppalanchi, S.; Anireddy, J. S.; Dwivedi, S.; Anantaraju, H. S.; Perumal, Y.; Sigalapalli, D. K.; Babu, B. N.; Ethiraj, K. S. Synthesis and α-glucosidase inhibition activity of dihydroxy pyrrolidines. *Bioorg. Med. Chem. Lett.* **2017**, *27*, 2818−2823.
(50) Oboh, G.; Ogunsuyi, O. B.; Ogunbadejo, M. D.; Adefegha, S. A. Influence of gallic acid on α-amylase and α-glucosidase inhibitory properties of acarbose. *J. Food Drug Anal.* **2016**, *24*, 627−634.
(51) Xue, N.; Jia, Y.; Li, C.; He, B.; Yang, C.; Wang, J. Characterizations and Assays of α-Glucosidase Inhibition Activity on Gallic Acid Cocrystals: Can the Cocrystals be Defined as a New Chemical Entity During Binding with the α-Glucosidase? *Molecules* **2020**, *25*, 1163.
(52) Montazeri, A. S.; Mohammadi, A.; Adib, N.; Naeemy, A. Development and Validation of a Stability-Indicating HPLC Method for the Determination of Acarbose in Pharmaceutical Dosage Forms. *J. Anal. Chem.* **2018**, *73*, 910−916.
(53) Granados-Guzmán, G.; Castro-Ríos, R.; de Torres, N. W.; Salazar-Aranda, R. Optimization and Validation of a Microscale In vitro Method to Assess α-Glucosidase Inhibition Activity. *Curr. Anal. Chem.* **2018**, *14*, 458−464.

https://doi.org/10.1021/acsami.1c02505
ACS Appl. Mater. Interfaces 2021, 13, 25624−25634